Preferential association with ClC-3 permits sorting of ClC-4 into endosomal compartments

Received for publication, June 13, 2017, and in revised form, September 15, 2017 Published, Papers in Press, September 26, 2017, DOI 10.1074/jbc.M117.801951

Raul E. Guzman[1], **Stefanie Bungert-Plümke, Arne Franzen, and Christoph Fahlke**[2]

From the Institute of Complex Systems, Zelluläre Biophysik (ICS-4), Forschungszentrum Jülich, 52425 Jülich, Germany

Edited by Roger J. Colbran

ClC-4 is an intracellular Cl^-/H^+ exchanger that is highly expressed in the brain and whose dysfunction has been linked to intellectual disability and epilepsy. Here we studied the subcellular localization of human ClC-4 in heterologous expression systems. ClC-4 is retained in the endoplasmic reticulum (ER) upon overexpression in HEK293T cells. Co-expression with distinct ClC-3 splice variants targets ClC-4 to late endosome/lysosomes (ClC-3a and ClC-3b) or recycling endosome (ClC-3c). When expressed in cultured astrocytes, ClC-4 sorted to endocytic compartments in WT cells but was retained in the ER in *Clcn3*$^{-/-}$ cells. To understand the virtual absence of ER-localized ClC-4 in WT astrocytes, we performed association studies by high-resolution clear native gel electrophoresis. Although other CLC channels and transporters form stable dimers, ClC-4 was mostly observed as monomer, with ClC-3–ClC-4 heterodimers being more stable than ClC-4 homodimers. We conclude that unique oligomerization properties of ClC-4 permit regulated targeting of ClC-4 to various endosomal compartment systems via expression of different ClC-3 splice variants.

ClC-3 and ClC-4 are chloride/proton exchangers that reside primarily in intracellular organelles (1, 2) of the brain, heart, skeletal muscle, and epithelia (3, 4). The functional relevance of ClC-3 and ClC-4 in the central nervous system is illustrated by pronounced hippocampal and retinal degeneration in *Clcn3*$^{-/-}$ knockout animal models (5–7) as well as by naturally occurring *CLCN4* mutations in patients with X-linked intellectual disability or epilepsy (8, 9). However, the cellular roles of ClC-3 and ClC-4 have remained insufficiently understood, mostly because of unclear subcellular localization of these two transport proteins.

The subcellular localization of ClC-4 was studied in multiple preparations, with conflicting results. Although Okkenhaug *et al.* (10) described endoplasmic reticulum (ER)[3] localization of ClC-4 upon heterologous expression in mammalian cells, endogenous ClC-4 inserts into the early endosomes and into the apical membrane of Caco-2 cells, a model system for human enterocytes (11). Moreover, ClC-4 contributes to acidification and to transferrin receptor trafficking in endosomes of CaCo-4, COS-7, and LLCPK-1 cells (12). These separate results might be due to the formation of heterodimers with other CLC transporters that target ClC-4 to intracellular compartments inaccessible to homodimers. Earlier reports have already described heterodimerization of ClC-4 with ClC-3 or ClC-5 (11, 13). ClC-5 targets to recycling endosomes (14), and alternative splicing of ClC-3 results in various localizations of different variants, including recycling endosomes (15), the Golgi (16), synaptic-like microvesicles (17), and synaptic vesicles (5, 18).

Here we investigated the subcellular localization of ClC-4 after expression in cultured mammalian cells. We observed targeting of ClC-4 into diverse endosomal pathways by forming heterodimeric assemblies with ClC-3 that are more stable than ClC-4 homodimers.

Results

Identification of sequence signals responsible for the subcellular targeting of ClC-4

Alternative splicing of *Clcn4* was reported to result in translation of two distinct ClC-4 isoforms that differ in the amino-terminal end of the protein (12), with a shorter splice variant (687 amino acids) lacking ~50% of helix A of ClC-4. Although expression of the long isoform as a fluorescent fusion protein in HEK293T cells generates robust whole-cell fluorescence levels and currents (amplitude at +175 mV, 1.20 ± 0.4 nA, $n = 5$) with defined time and voltage dependences in whole-cell patch clamp experiments (1, 2, 19), we observed significantly reduced expression levels and absent whole-cell currents in cells expressing the short isoform (at +175 mV, 0.03 ± 0.04 nA, $n = 11$). Because all functional CLC channels and transporters exhibit an intact helix A and because we were unable to express the short ClC-4 isoform at comparable protein levels as other constructs, we restricted ourselves to the long ClC-4 in the following analyses.

The long ClC-4 splice variant is mostly localized to the endoplasmic reticulum, with a subcellular distribution that overlaps with the ER marker Bcl-2 (Manders coefficient (MC) = 0.81 ± 0.02, $n = 9$) and only little with the lysosomal marker LAMP1 (MC = 0.13 ± 0.02, $n = 10$) (Fig. 1, *A* and *E*). We recently reported that a closely related transporter, the ClC-3 splice variant ClC-3a, localizes to the late endosomal/lysosomal system and that its expression in mammalian cells results in a characteristic lysosomal enlargement that is easy to distinguish from

The authors declare that they have no conflicts of interest with the contents of this article.

[1] To whom correspondence may be addressed. E-mail: r.guzman@fz-juelich.de.

[2] To whom correspondence may be addressed: E-mail: c.fahlke@fz-juelich.de.

[3] The abbreviations used are: ER, endoplasmic reticulum; MC, Manders coefficient; aa, amino acids; eGFP, enhanced GFP; hrCNE, high-resolution clear native gel electrophoresis; MBP, maltose-binding protein; mYFP, monomeric YFP; mRFP, monomeric red fluorescent protein; Tricine, *N*-[2-hydroxy-1,1-bis(hydroxymethyl)ethyl]glycine.

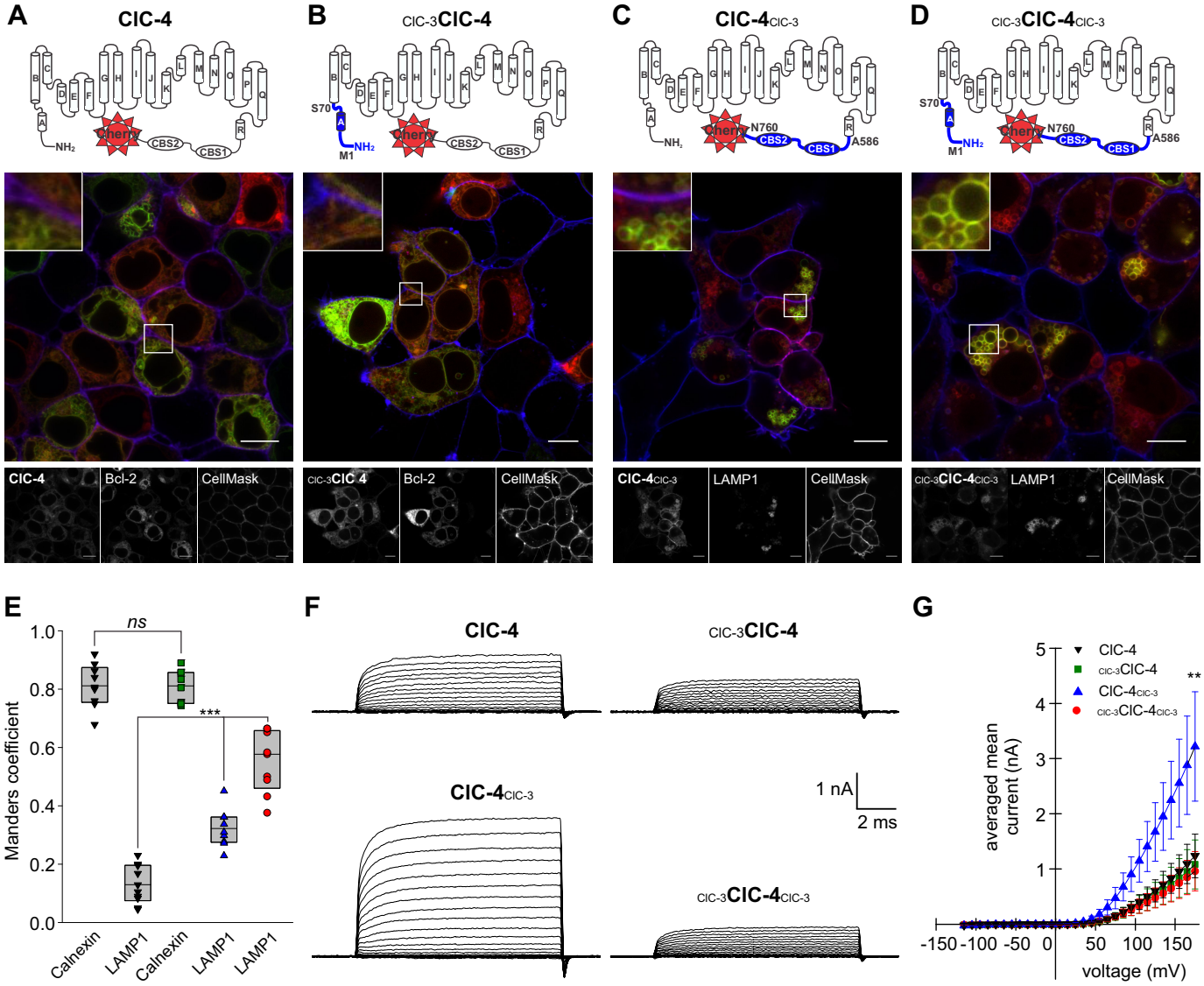

Figure 1. Transplanting the carboxyl terminus from ClC-3a modifies intracellular localization of ClC-4. *A–D*, confocal images of HEK293T cells heterologously expressing ClC-4, $_{ClC-3}$ClC-4, ClC-4$_{ClC-3}$, or $_{ClC-3}$ClC-4$_{ClC-3}$ and the corresponding protein topology schematics illustrating the different protein domains that were exchanged (*blue*). For confocal images, cells were either cotransfected with the ER marker Bcl-2 or the lysosomal marker LAMP1 and stained with the plasma membrane marker CellMask^{TM}. *Scale bars* = 10 μm. *E*, box plot of Manders coefficients of the co-localization analysis between ClC-4 chimeric proteins and the corresponding intracellular marker (ClC-4/calnexin, $n = 9$; ClC-4/Lamp1, $n = 10$; $_{ClC-3}$ClC-4/calnexin, $n = 8$; ClC-4$_{ClC-3}$/Lamp1, $n = 9$; $_{ClC-3}$ClC-4$_{ClC-3}$/Lamp1, $n = 9$; with n being the number of fields of view with at least three to five co-transfected cells. The MC values for ClC-4$_{ClC-3}$/Lamp1 and $_{ClC-3}$ClC-4$_{ClC-3}$/Lamp1 were significantly different from values in cells expressing ClC-4/Lamp1. *F*, representative whole-cell recordings from HEK293T cells expressing ClC-4 or its mutant variants. *G*, voltage dependence of mean current amplitudes for cells expressing WT or various mutant ClC-4 constructs obtained from recordings as shown in *F* (ClC-4, $n = 5$; $_{ClC-3}$ClC-4, $n = 5$; ClC-4$_{ClC-3}$, $n = 5$; $_{ClC-3}$ClC-4$_{ClC-3}$, $n = 5$). Values are given as means ± S.D., with n giving the number of cells (**, $p < 0.01$; ***, $p < 0.001$; *t* test; *ns*, not significant).

the ER localization of ClC-4 (2). To identify sequence motifs that are responsible for ER retention of ClC-4, we employed a chimera approach with ClC-4 and ClC-3a. We transplanted either the complete amino terminus (until the start of the B helix, $_{ClC-3}$ClC-4) or the complete carboxyl terminus (starting with the end of the R helix, ClC-4$_{ClC-3}$) or both ($_{ClC-3}$ClC-4$_{ClC-3}$) from ClC-3a to ClC-4 (Fig. 1) or vice versa (Fig. 2) and studied the subcellular distribution with confocal imaging in transfected HEK293T cells. Whereas the expression of the chimeric protein $_{ClC-3}$ClC-4 shows a similar subcellular distribution as ClC-4 (Fig. 1*B*, colocalization with Bcl-2, MC = 0.81 ± 0.02, $n = 8$, $p = 0.93$, *t* test) (Fig. 1*E*), we observed large vesicular structures in cells expressing $_{ClC-3}$ClC-4$_{ClC-3}$. The additional substitution of the ClC-3 carboxyl terminus significantly increased the degree of colocalization with the lysosomal marker LAMP1 (MC ($_{ClC-3}$ClC-4$_{ClC-3}$) = 0.55 ± 0.03, $n = 9$, $p \leq 0.001$) (Fig. 1, *D* and *E*). ClC-4$_{ClC-3}$ displays significant surface membrane insertion in addition to lysosomal localizations (MC (ClC-4$_{ClC-3}$/LAMP1) = 0.32 ± 0.02, $n = 9$, $p \leq 0.001$) (Fig. 1, *C* and *E*).

We next performed electrophysiological recordings on WT and chimeric transporters. All tested chimeras with a ClC-4 background display voltage-dependent changes in current amplitudes that closely resemble ClC-4, *i.e.* prominent time-dependent increases in current amplitudes upon depolarizing voltage steps (1, 2, 20). Neither $_{ClC-3}$ClC-4 or $_{ClC-3}$ClC-4$_{ClC-3}$

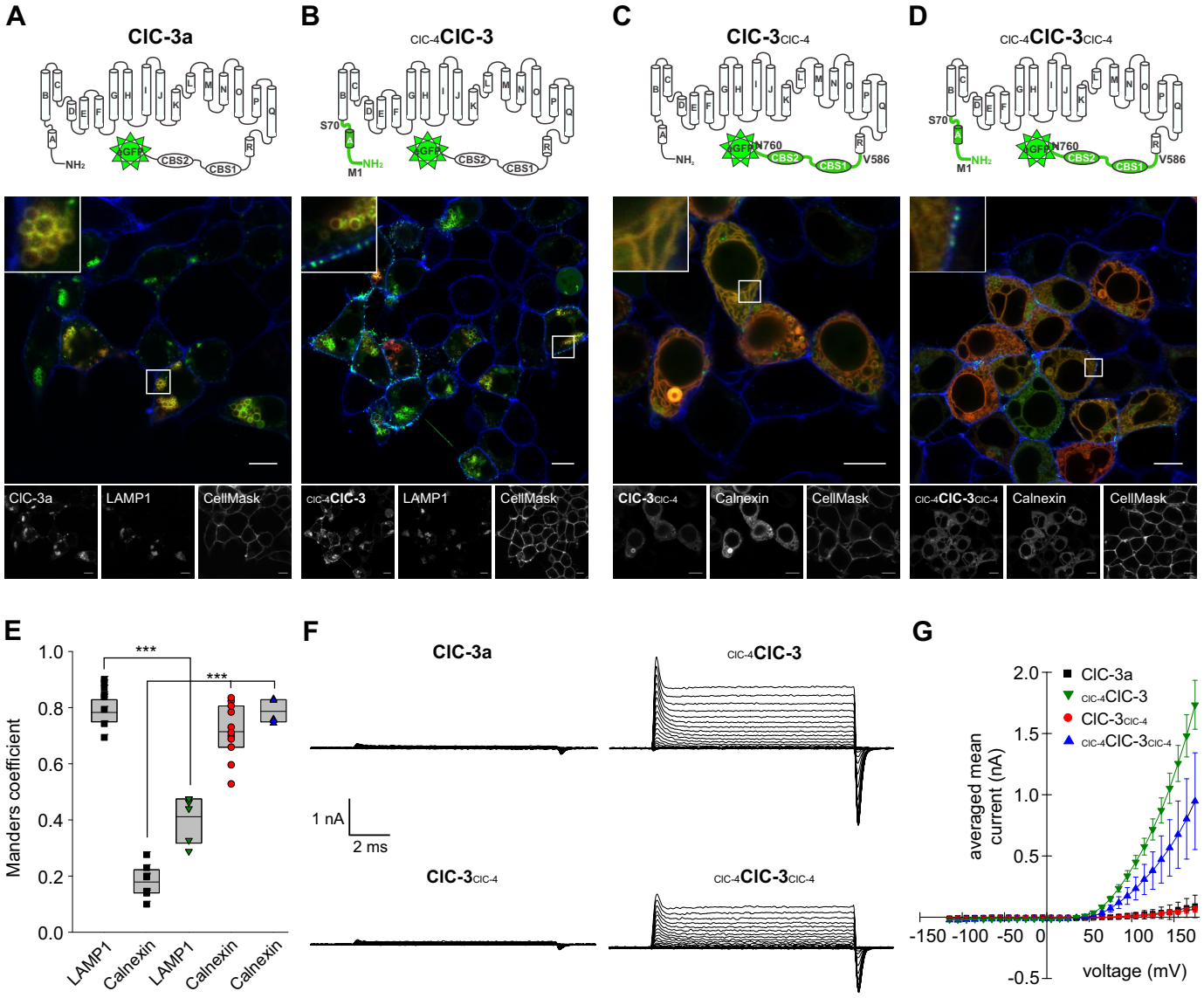

Figure 2. Transplanting the ClC-4 amino and carboxyl termini redirects ClC-3a to the endoplasmic reticulum. *A–D*, confocal images of HEK293T cells heterologously expressing ClC-3, $_{ClC\text{-}4}$ClC-3, ClC-3$_{ClC\text{-}4}$, or $_{ClC\text{-}4}$ClC-3$_{ClC\text{-}4}$ and the corresponding protein topology pictures to show part of the protein sequence that was substituted (*green*). For confocal images, cells were either cotransfected with the ER marker calnexin or the lysosomal marker LAMP1. *Scale bars* = 10 μm. *E*, box plot of Manders coefficients of the co-localization analysis for ClC-3 chimeric proteins and corresponding intracellular marker (ClC-3a/LAMP1, n = 8; ClC-3/Calnexin, n = 7; $_{ClC\text{-}4}$ClC-3/LAMP1, n = 6; ClC-3$_{ClC\text{-}4}$/Calnexin, n = 11; $_{ClC\text{-}4}$ClC-3$_{ClC\text{-}4}$/Calnexin, n = 5), with n being the number of fields of view containing at least three to five co-transfected cells. All ClC-3a chimeric constructs show MC values that were significantly different from those measured in ClC-3a. *F*, representative whole-cell recordings from HEK293T cells expressing ClC-3 or its mutant variants. *G*, voltage dependence of mean current amplitudes for cells expressing WT or various ClC constructs obtained from recordings as shown in *F* (ClC-3a, n = 4; $_{ClC\text{-}4}$ClC-3, n = 8; ClC-3$_{ClC\text{-}4}$, n = 4; $_{ClC\text{-}4}$ClC-3$_{ClC\text{-}4}$, n = 6). Values are given as means ± S.D., with n giving the number of cells. ***, $p < 0.001$, t test.

nor ClC-4$_{ClC\text{-}3}$ exhibit capacitive currents with amplitudes corresponding to ClC-3 (2). Differences in the subcellular distribution are reflected by distinct macroscopic current amplitudes (at +175 mV, ClC-4 = 1.20 ± 0.04 nA, n = 5, $_{ClC\text{-}3}$ClC-4 = 1.09 ± 0.4 nA, n = 5, $_{ClC\text{-}3}$ClC-4$_{ClC\text{-}3}$ = 1.00 ± 0.35 nA, n = 5, ClC-4$_{ClC\text{-}3}$ = 3.22 ± 0.9 nA, n = 5; Fig. 1, *F* and *G*). Whole-cell currents exclusively originate from transporters in the surface membrane and thus report on changes in the numbers of transporter with this localization. Because altered expression levels also have a direct impact on transporter numbers in all subcellular compartments, whole-cell currents do not only reflect the ability of the expressed transporter to insert into the plasma membrane and in the individual transport rates but also depend on protein expression levels, which are often affected by alterations in the primary sequence. Changes in whole-cell currents thus only provide a qualitative measure for surface membrane insertion of the tested transporter chimeras. However, the subcellular localization of WT ClC-3a prevents measurable surface insertion under all expression levels obtained so far. Thus, current amplitudes exceeding background currents are a clear indication for a change in subcellular localization in a chimera approach using ClC-3a and ClC-4.

Transplanting the carboxyl terminus of ClC-3 (ClC-4$_{ClC\text{-}3}$) increases surface membrane insertion (Fig. 1*C*) and macroscopic current amplitudes (Fig. 1*F*) to values above WT ClC-4 (Fig. 1, *F* and *G*). In agreement with their subcellular localiza-

tion to the endoplasmic reticulum or lysosomes, $_{ClC\text{-}3}$ClC-4 and $_{ClC\text{-}3}$ClC-$4_{ClC\text{-}3}$ currents (Fig. 1, *B* and *D–G*) are significantly smaller than currents observed in cells expressing ClC-$4_{ClC\text{-}3}$ ($p = 0.002$) (Fig. *1*, *F* and *G*). Fig. 2 summarizes the results of ClC-3-based chimeras. WT ClC-3a is mainly localized to lysosomes (MC for co-localization with LAMP1, 0.82 ± 0.02, $n = 8$) (Fig. 2, *A* and *E*), and the absence of surface membrane insertion of ClC-3a prevents recording of specific currents in transfected cells (at +175 mV, ClC-3 = 0.10 ± 0.09 nA, $n = 4$; Fig. 2, *F* and *G*). $_{ClC\text{-}4}$ClC-3 and $_{ClC\text{-}4}$ClC-$3_{ClC\text{-}4}$ both insert into the surface membrane and give rise to transport currents that resemble those of mutant ClC-3a, in which an amino-terminal dileucine motif was removed (at +175 mV, $_{ClC\text{-}4}$ClC-3 = 1.73 ± 0.02 nA, $n = 6$, $_{ClC\text{-}4}$ClC-$3_{ClC\text{-}4}$ = 0.90 ± 0.04 nA, $n = 6$; Fig. 2, *B*, *D*, *F*, and *G*) (2, 15). Confocal images demonstrate surface membrane/lysosome localization of $_{ClC\text{-}4}$ClC-3 (Fig. 2, *B* and *E*) and ER localization of $_{ClC\text{-}4}$ClC-$3_{ClC\text{-}4}$ (Fig. 2, *D* and *E*). In addition to its occurrences in large lysosomal vesicular structures typical for WT ClC-3a (Fig. 2, *A* and *E*), ClC-$3_{ClC\text{-}4}$ is localized in the ER (Fig. 2, *C* and *E*). Current amplitudes were largest for $_{ClC\text{-}4}$ClC-3 (Fig. 2*F*), followed by $_{ClC\text{-}4}$ClC-$3_{ClC\text{-}4}$ (Fig. 2*F*). The predominant intracellular localization of ClC-$3_{ClC\text{-}4}$ results in the virtual absence of macroscopic current amplitudes (at +175 mV, 0.10 ± 0.02 nA, $n = 6$; Fig. 2, *F* and *G*).

Transplanting the ClC-3 carboxyl terminus to ClC-4 promotes surface membrane insertion, as shown in the confocal images, and furthermore increases macroscopic current amplitudes (Fig. 1, *C*, *F*, and *G*), whereas the inverse chimera, ClC-$3_{ClC\text{-}4}$, targets to the endoplasmic reticulum (Fig. 2, *C* and *E–G*). Exchanging the ClC-3 amino terminus with its ClC-4 counterpart removes a clathrin-binding dileucine motif (20, 21) so that $_{ClC\text{-}4}$ClC-3 can insert into the surface membrane (Fig. 2, *B*, *F*, and *G*). Taken together, these results indicate that ClC-4 lacks the endosomal targeting sequences of ClC-3 and that a carboxyl-terminal ER retention signal is responsible for the subcellular localization of ClC-4.

The endoplasmic reticulum retention signal of ClC-4 is located in the interlinker between CBS1 and CBS2

The carboxyl terminal tails of CLC channels and transporters contain two CBS domains (22–24) that are flanked by flexible linker regions. We generated three additional chimeras between ClC-3a and ClC-4 to further narrow down the localization of ClC-4 ER retention signals: ClC-$3_{ClC\text{-}4(586-611aa)}$, exchanging the linker between the R helix and CBS1; ClC-$3_{ClC\text{-}4(CBS1\text{-}Linker)}$, transplanting CBS1 and the linker between the two CBS domains; and ClC-$3_{ClC\text{-}4(CBS2-760aa)}$, with exchanged CBS2 and a distal carboxyl terminus (Fig. 3, *A–C*). Although ClC-$3_{ClC\text{-}4(586-611aa)}$ (Fig. 3, *A* and *G*) and ClC-$3_{ClC\text{-}4(CBS2-760aa)}$ (Fig. 3, *C* and *G*) left endosomal localization unaffected, we observed prominent ER staining in cells expressing ClC-$3_{ClC\text{-}4(CBS1\text{-}Linker)}$ (MC (calnexin) = 0.57 ± 0.03, $n = 8$, Mann-Whitney rank-sum-test, $p \leq 0.001$) (Fig. 3, *B* and *G*).

We next constructed three inverse chimeras by exchanging sequence regions from ClC-3 to ClC-4: ClC-$4_{ClC\text{-}3(CBS1\text{-}Linker)}$, ClC-$4_{ClC\text{-}3(CBS1)}$, and ClC-$4_{ClC\text{-}3(Linker)}$. Transplanting CBS1 alone (ClC-$4_{ClC\text{-}3(CBS1)}$) does not modify the ER localization of ClC-4 (Fig. 3, *D* and *G*). In contrast, exchanging the CBS linker region, either alone (ClC-$4_{ClC\text{-}3(Linker)}$) or together with CBS 1 (ClC-$4_{ClC\text{-}3(CBS1\text{-}Linker)}$), results in preferential insertion into the surface membrane with additional intracellular staining (Fig. 3, *E–G*), (MC (ClC-$4_{ClC\text{-}3(CBS1\text{-}Linker)}$/calnexin) = 0.39 ± 0.03, $n = 7$; MC (ClC-$4_{ClC\text{-}3(CBS1\text{-}Linker)}$/CellMask) = 0.38 ± 0.02, $n = 7$; MC (ClC-$4_{ClC\text{-}3(Linker)}$/calnexin) = 0.27 ± 0.02, $n = 13$; MC (ClC-$4_{ClC\text{-}3(Linker)}$/CellMask) = 0.47 ± 0.02, $n = 13$).

Removal of this signal resulted in ER exit and surface membrane insertion of ClC-4, increased the macroscopic current amplitudes (at +175 mV, ClC-$4_{ClC\text{-}3(Linker)}$ = 2.73 ± 0.70 nA, $n = 5$), and its insertion into ClC-3 promote ER retention (data not shown). We conclude that the CBS linker region contains the ER retention signal of ClC-4.

Heterodimerization enables endosomal localization of ClC-4

In the past, various channel/transporter families have been identified in which hetero-oligomerization permits targeting of proteins to particular subcellular localizations (25, 26). ClC-4 is known to heterodimerize with other CLC transporters (14); however, the consequences of subcellular localization have not been studied before. Fig. 4 depicts confocal images from cells co-expressing ClC-4 with ClC-3a (Fig. 4*A*), ClC-3b (Fig. 4*B*), ClC-3c (Fig. 4*C*), or ClC-6 (Fig. 4*D*). Co-expressing ClC-3 variants abolishes endoplasmic reticulum localization of ClC-4. ClC-4 localizes to large endosomal structures when co-expressed with ClC-3a or ClC-3b (Fig. 4, *A* and *B*) but is preferentially present in small vesicle-like structures that localize close to the plasma membrane in cells co-expressing ClC-4 with ClC-3c (Fig. 4*C*). In contrast, ClC-4 and ClC-6 do not co-localize (MC = 0.16 ± 0.06, $n = 9$), and ClC-4 retains its endoplasmic reticulum localization when co-expressed with ClC-6 (Fig. 4, *D* and *E*). We observed high co-localization coefficients in cells co-expressing ClC-4-mCherry and eGFP fusion proteins of ClC-3a, ClC-3b, or ClC-3c (MC (ClC-4/ClC-3a) = 0.79 ± 0.10, $n = 8$; MC (ClC-4/ClC-3b) = 0.75 ± 0.10, $n = 9$; MC (ClC-4/ClC-3c) = 0.72 ± 0.10, $n = 12$; Fig. 4*E*). We conclude that ClC-4 associates with ClC-3 and that trafficking of the heterodimer is controlled by endosomal trafficking signals of ClC-3.

To further test the concept of ClC-4 sorting via association with ClC-3, we employed primary astrocytic cultures from *Clcn3*$^{-/-}$ animals (5) and compared them with WT cells. Fig. 5 shows confocal images from WT (Fig. 5*A*) and *Clcn3*$^{-/-}$ (Fig. 5*B*) astrocytes co-transduced with fluorescent ClC-4 fusion protein and Rab7-mRFP via lentiviral gene transfer (27). Whereas WT astrocytes exhibit punctuate staining and show colocalization with the late endosomal/lysosomal marker Rab7 (MC = 0.70 ± 0.1, $n = 19$) (Fig. 5, *A* and *C*), ClC-4 predominantly localizes to the ER in *Clcn3*$^{-/-}$ cells (Fig. 5, *B* and *C*) without colocalization with Rab7 (MC = 0.13 ± 0.05, $n = 6$). These differences in the subcellular distribution of ClC-4 are not due to increased expression levels in *Clcn3*$^{-/-}$ astrocytes Fig. 5*D*). Thus, these results further support the notion that ClC-3 controls intracellular trafficking of ClC-4.

ClC-4 exhibits unique oligomerization behavior

Co-expression studies in mammalian cell cultures (Fig. 4) as well as the experiments in cultured astrocytes (Fig. 5) reveal an

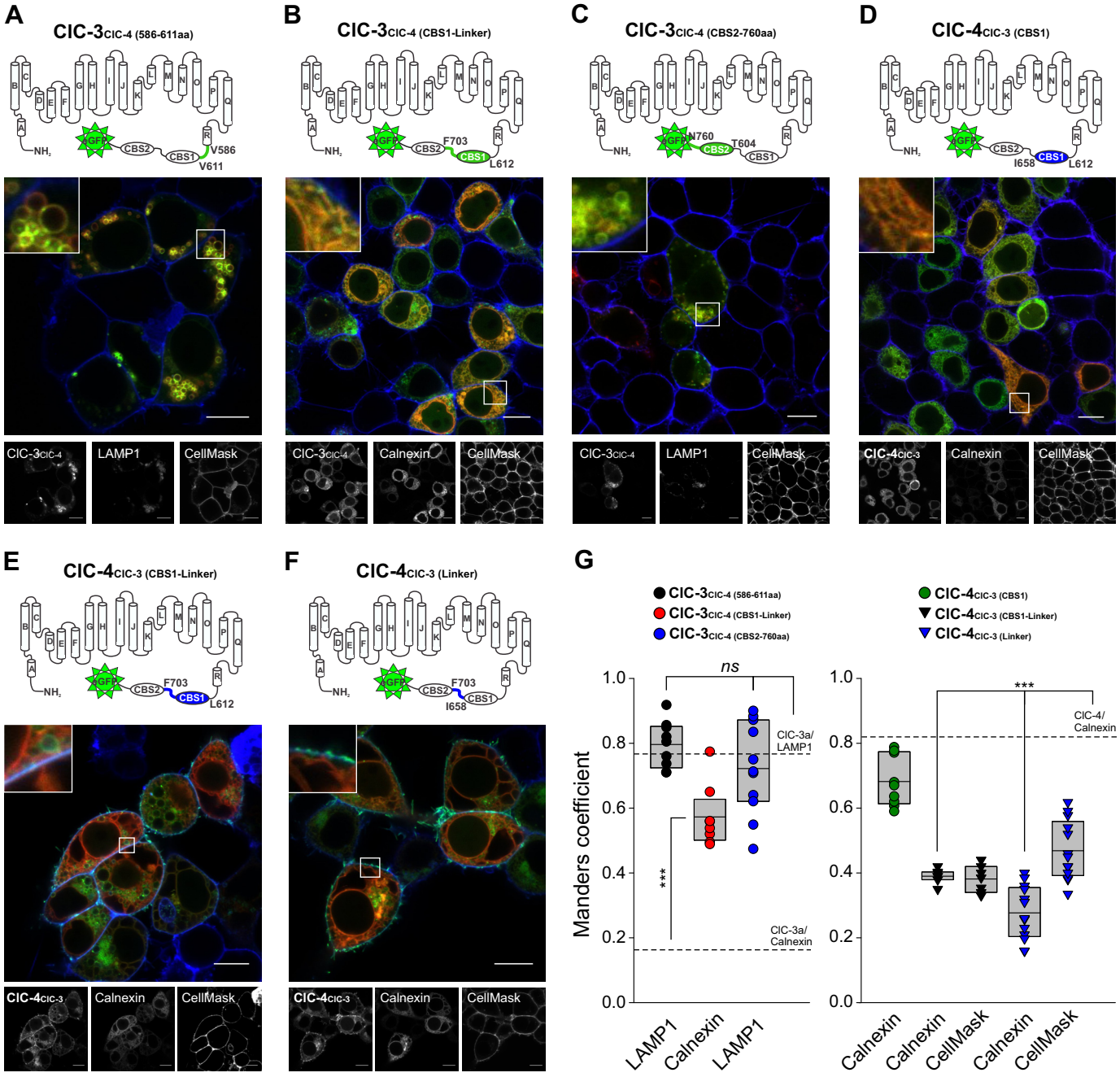

Figure 3. The endoplasmic reticulum retention signal of ClC-4 is located in the interlinker between CBS1 and CBS2. *A–F*, confocal images of HEK293T cells heterologously expressing ClC-3a or ClC-4 chimeric constructs: ClC-$3_{ClC\text{-}4(586-611aa)}$, ClC-$3_{ClC\text{-}4\ (CBS1\text{-}Linker)}$, or ClC-$3_{ClC\text{-}4(CBS2-760aa)}$ (*A–C*) or ClC-$4_{ClC\text{-}3(CBS1)}$, ClC-$4_{ClC\text{-}3(CBS1\text{-}Linker)}$, or ClC-$4_{ClC\text{-}3(Linker)}$ (*D–F*). In the protein topology image, exchanged protein sequences are highlighted in *green* or *blue*. Cells were either co-transfected with the ER markers calnexin/Bcl-2 or the lysosomal marker LAMP1. *Scale bars* = 10 μm. *G*, box plot of Manders coefficients of the co-localization analysis for ClC-3a or ClC-4 chimeric proteins with the corresponding intracellular marker (ClC-$3_{ClC\text{-}4(586-611aa)}$/LAMP1, $n = 9$; ClC-$3_{ClC\text{-}4(CBS1\text{-}Linker)}$/calnexin, $n = 8$; ClC-$3_{ClC\text{-}4(CBS2-760aa)}$/LAMP1, $n = 11$; or ClC-$4_{ClC\text{-}3(CBS1)}$/calnexin, $n = 10$; ClC-$4_{ClC\text{-}3(CBS1\text{-}Linker)}$/calnexin, $n = 7$; or ClC-$4_{ClC\text{-}3(CBS1\text{-}Linker)}$/CellMask, $n = 7$; ClC-$4_{ClC\text{-}3(Linker)}$/calnexin, $n = 13$; or ClC-$4_{ClC\text{-}3(Linker)}$/CellMask, $n = 13$), with *n* being the number of fields of view containing at least three to five co-transfected cells. *Dashed lines* correspond to the average values obtained for ClC-3a/LAMP1 or ClC-3a/calnexin (*left panel*) and ClC-4/calnexin (*right panel*). MC values from ClC-$3_{ClC\text{-}4(586-611aa)}$/LAMP1 and ClC-$3_{ClC\text{-}4(CBS2-760aa)}$/LAMP1 were not significantly different from the control ClC-3a/LAMP1 (*t* test, $p = 0.48$). In contrast, ClC-$3_{ClC\text{-}4(CBS1\text{-}Linker)}$ exhibits significantly higher MCs with calnexin than ClC-3a/calnexin (Mann-Whitney rank-sum test, $p \leq 0.001$). ClC-$4_{ClC\text{-}3(CBS1\text{-}Linker)}$ and ClC-$4_{ClC\text{-}3(CBS1\text{-}Linker)}$ show significantly lower MCs than ClC-4/calnexin (***, $p < 0.001$; *t* test; *ns*, not significant).

almost complete change in subcellular localization of ClC-4 in the presence of ClC-3. Although HEK293T cells expressing ClC-4 alone show prominent ER staining, there is virtually no ER fluorescence staining in cells co-expressing ClC-4 together with various ClC-3 isoforms. This is at first glance surprising. CLC channels and transporters are dimers, and co-expression of ClC-3 and ClC-4 is expected to result in the appearance of ClC-3 and ClC-4 homodimeric as well as ClC-3–ClC-4 heterodimeric transporters. In the case of equal association probabilities, homo- and heterodimeric transporters will be binomially distributed, and comparable expression levels of ClC-3 and ClC-4 in co-transfected HEK293T cells thus predict 25% ClC-4

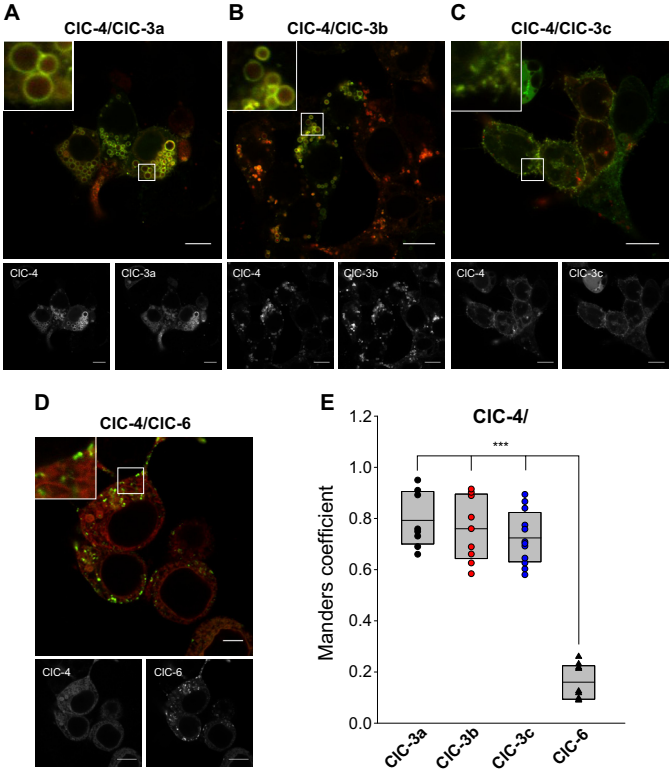

Figure 4. ClC-4 is targeted to distinct endosomal compartments when co-transfected with interacting CLC transporters. *A–D*, confocal images of HEK293T cells co-expressing ClC-4 and ClC-3a (*A*), ClC-3b (*B*), ClC-3c (*C*), or ClC-6 (*D*). *Scale bars* = 10 μm. *E*, box plot of Manders coefficients of the co-localization analysis for ClC-4 and various other CLC transporters (ClC-4/ClC-3a, $n = 8$; ClC-4/ClC-3b, $n = 9$; ClC-4/ClC-3c, $n = 12$; ClC-4/ClC-6, $n = 9$), with n being the number of fields of view containing at least three to five co-transfected cells. Co-localization analysis shows that cells co-expressing ClC-4 and different ClC-3 splice variants exhibit similar MC values but significantly larger coefficients than cells co-expressing ClC-4 and ClC-6. ***, $p < 0.001$; *t* test).

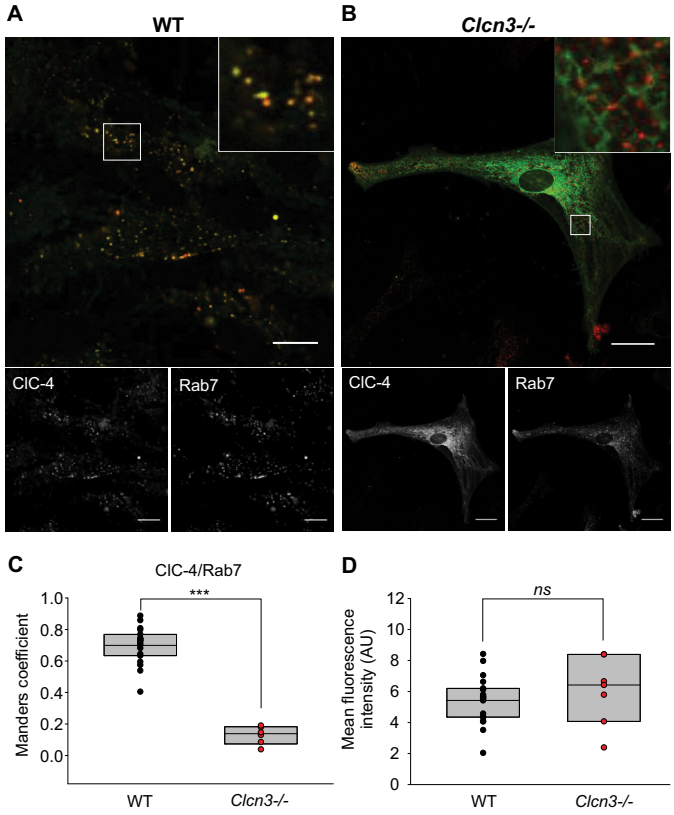

Figure 5. Different subcellular ClC-4 distributions in WT and *Clcn3*$^{-/-}$ astrocytes. *A* and *B*, confocal images of astrocytes from WT (*A*, *scale bar* = 10 μm) or *Clcn3*$^{-/-}$ (*B*, *scale bar* = 30 μm) mice co-transduced with fluorescent ClC-4 fusion proteins and the late endosomal/lysosomal marker Rab7 via lentiviral gene transfer. *C*, box plot of Manders coefficients of the co-localization analysis for ClC-4 and Rab7 in WT or *Clcn3*$^{-/-}$ astrocytes. MC values are significantly different for WT and *Clcn3*$^{-/-}$ astrocytes ($p < 0.001$; *t* test). *D*, box plot of mean whole-cell fluorescence intensity of WT ($n = 19$) or *Clcn3*$^{-/-}$ ($n = 7$) cells expressing ClC-4 fusion proteins (n, number of analyzed fields of view containing at least three to five cells; *AU*, arbitrary unit; *ns*, not significant).

homodimers. The absence of ER staining in co-transfected HEK293T cells thus suggests the preferential association of ClC-4 with ClC-3.

To test for differences in homo- and heterodimeric assembly rates, we studied oligomerization by high-resolution clear native gel electrophoresis (hrCNE) (28, 29). The similarity of molecular masses makes the distinction of ClC-3b (91 kDa) and ClC-4 (84 kDa) by gel electrophoresis difficult. We therefore increased the size of fluorescently tagged ClC-3 by covalently attaching a maltose-binding protein (MBP) moiety (42.5 kDa) to the amino terminus. Subcellular distribution and transport properties of MBP-ClC-3b were assessed by confocal microscopy and by patch clamp recordings and found not to be affected by the maneuver (data not shown). ClC-3 and ClC-4 are both glycosylated (30), and the co-existence of multiple glycosylation states causes rather unfocused protein bands, making assignment of distinct protein conformations in hrCNE difficult. To reduce protein glycosylation, we mutated the asparagines at positions Asn-880 and Asn-883 in MBP-ClC-3b and at Asn-428 and Asn-431 in ClC-4 to glutamine.

Transporters were resolved by SDS-PAGE and hrCNE from whole-cell lysates and visualized by scanning the gels after expressing MBP-ClC-3b-eGFP or ClC-4-eGFP either individually or together in mammalian cells (Fig. 6). SDS-PAGE was used to compare relative expression levels, indicating similar expression levels of MBP-ClC-3b and ClC-4 under all tested conditions (Fig. 6*A*). When expressed alone, ClC-3 shows two distinct bands in hrCNE (Fig. 6*B*), a monomeric and a homodimeric band. In contrast, we observed a predominantly monomeric band with a faint homodimeric band in experiments expressing ClC-4 alone. In co-expression experiments, the formation of heterodimers produces a yellow band because of overlapping of ClC-4-mCherry and MBP-ClC-3-eGFP fluorescences (Fig. 6*B*).

A limitation of native gel electrophoresis in determining the native oligomeric state of proteins and in quantifying the stability of such oligomers is that solubilization steps might dissociate protein–protein interactions that exist in native membranes. We tested subunit association of the muscle chloride channel ClC-1 (31) as a control and resolved YFP-ClC-1 as a single dimer band in hrCNE (Fig. 6*B*) (32, 33). This result demonstrates that solubilization and gel electrophoresis can conserve CLC dimers and that the different observed monomer/dimer ratios are due to isoform-specific properties. However, it appears possible that the percentage of ClC-4 monomers is lower in native systems than after solubilization.

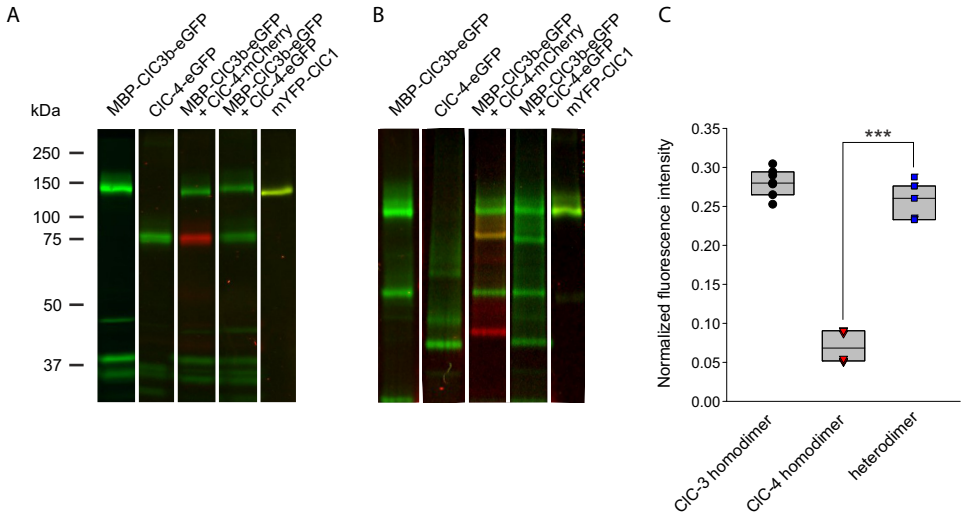

Figure 6. hrCNE demonstrates different stabilities of ClC-1, ClC-3, and ClC-4 homodimers. *A*, SDS-PAGE analysis of fluorophore-tagged proteins heterologously expressed in HEK 293T cells. *B*, hrCNE analysis of the same proteins. Fluorophore-tagged proteins were visualized by fluorescence scanning of the gels, respectively. *C*, box plot of the normalized fluorescence intensities of the protein bands assigned to homodimeric or heterodimeric bands. Normalization was performed as described under "Experimental Procedures." *MBP-ClC3b-eGFP*, His-MBP-ClC-3b-eGFP N880/883Q; *ClC4-eGFP*, His-ClC-4-eGFP N428/431Qn; *ClC4-mCherry*, His-ClC-4-mChery N428/431Q. Data were obtained from seven independent experiments. $p \leq 0.001$, Mann-Whitney rank-sum test.

Fig. 6*C* shows normalized fluorescence intensities of hrCNE gel lanes containing ClC-3 or ClC-4 homodimers or ClC-3/ClC-4 heterodimers from co-expression experiments. Normalized values are proportional to the relative amount of the fluorescent fusion proteins (34, 35) in different oligomeric states and thus illustrate differences in the stability of these oligomers. A comparison of these values demonstrates significantly lower amounts of ClC-4 homodimer but comparable amounts of ClC-3 homodimer and ClC-3–ClC-4 heterodimer. We conclude that ClC-4 homodimers are less stable than ClC-3 homodimers and less stable than ClC-3–ClC-4 heterodimers.

Discussion

ClC-3 and ClC-4 are two closely related intracellular chloride/proton exchangers that co-exist in neurons, glia, muscle, heart, and epithelial cells (3, 5, 7, 36, 37). Both mediate outwardly rectifying transport currents with significant currents only at very positive potentials (1, 2, 15, 19, 38, 39). ClC-3 and ClC-4 both perform incomplete transport cycles that result in capacitive currents (2); however, there are significant differences in the relative number of complete and incomplete cycles. Although ClC-3 mainly performs such non-transporting cycles, ClC-4 is an effective coupled transporter with more than 10-fold larger transport efficiency. Despite its apparently low transport efficiency, genetic ablation of ClC-3 results in pronounced neurodegeneration in *Clcn3*$^{-/-}$ animals (5–7). The consequences of ClC-4 ablation are rather benign (40), possibly because of the existence of functionally equivalent CLC transporters that are able to compensate for lacking ClC-4 transporters.

Targeting of ClC-4 into endosomal compartments by associated ClC-3 explains the distinct phenotypes of *Clcn3*$^{-/-}$ and *Clcn4*$^{-/-}$. Although ClC-4 homodimers are retained in the endoplasmic reticulum (Figs. 1 and 2), co-transfection of ClC-4 with distinct ClC-3 splice variants results in complete translocation into the particular subcellular compartment (Fig. 4). Whereas homodimers of various *Clcn3* splice variants mediate chloride/proton exchange in the Golgi, recycling early and late endosomes in *Clcn4*$^{-/-}$ cells, ClC-4 will remain in the ER of *Clcn3*$^{-/-}$ cells. Our results suggest that expression of separate ClC-3 splice variants or other CLC transporters will result in cell type-specific trafficking and localization of ClC-4 (1, 10–12).

Although predominantly localized to the endoplasmic reticulum, a fraction of homodimeric ClC-4 also inserts into the surface membrane in heterologous systems (1, 2, 15, 19, 38, 39). In native cells, homodimerization and/or heterodimerization with ClC-3c may permit insertion into the plasma membrane (11). In contrast, other ClC-3 splice variants, such as ClC-3a and ClC-3b, are exclusively present in late endosomal vesicles without any measurable number of transporters in the surface membrane (15). We took advantage of distinct intracellular trafficking of ClC-3a and ClC-4 in a chimera approach to elucidate molecular determinants of intracellular targeting (Figs. 1 and 2). Despite measurable surface membrane insertion of ClC-3c and ClC-4 transporters, the main physiological function of ClC-3 and ClC-4 is assumed to be transport across intracellular membranes (41).

CLC channels and transporters are generally assumed to form dimers in which each subunit functions independently of its counterpart (42, 43). In the *Escherichia coli* ClC, mutations have been identified that weaken the dimerization equilibrium and result in the formation of stable and functional monomers that are in dynamic equilibrium with dimeric transporters (44, 45). Our experiments demonstrate that ClC-4 does not form stable dimers, likely resembling the behavior of such engineered monomeric CLCs. We compared relative amounts of homo- and heterodimeric ClC-3 and ClC-4 by hrCNE PAGE and found that ClC-4 is a rather unstable dimer. Comparison of the intracellular chloride/proton exchangers ClC-3 and ClC-4 with the muscle chloride channel ClC-1 illustrates a much

higher stability of ClC-1 dimers. This may prevent the formation of ClC-1–ClC-4 heterodimers in skeletal muscle.

ClC-4 is more likely to oligomerize with ClC-3 than with another ClC-4 subunit (Fig. 6). This particular property of CLC transporters provides a potential biological significance of the co-existence and the different transport efficiencies of ClC-3 and ClC-4. In the absence of ClC-3, ClC-4 either remains monomeric or forms homodimers that are retained in the endoplasmic reticulum. With rising numbers of ClC-3, the number of ClC-3–ClC-4 in distinct target compartments will increase, resulting in significantly enhanced chloride/proton exchange in this particular cell organelle. However, at a certain expression level, homodimeric ClC-3 will start to dominate. At this point, chloride/proton transport will decrease and reach significantly lower transport rates at very high numbers of ClC-3 subunits. Because alternative splicing results in the translation of different ClC-3 isoforms with separate intracellular targeting (16), this mechanism will also permit regulation of the ClC-4 distribution between recycling endosomes, lysosome, synaptic vesicle, and Golgi by varying ClC-3 isoform expression.

Ion channels and transporters are usually assumed to exist as stable oligomers that are formed immediately after translation. In the case of the superfamily of voltage-gated cation channels, the subunits jointly form a central ion conduction pathway and are unstable as a monomer. The double-barreled architecture permits folding and function of monomeric CLC channels and transporters, and this feature is also the basis for dynamic equilibria between monomers and dimers (45). Here we report the physiological consequences of an extreme example of such dynamic oligomerization. ClC-4 cannot form stable homodimers and exists therefore mainly in heterodimeric assemblies with ClC-3 that dictate its subcellular localization.

Experimental procedures

Construction of expression plasmids and heterologous expression

cDNAs encoding full-length mouse ClC-3a, ClC-3b, or ClC-3c (15), full-length human ClC-4 (19), and full-length human ClC-6 (46) (kindly provided by Dr. J. Eggermont, Leuven, Belgium) were cloned into FsY1.1 G.W. or p156rrL vectors (kindly provided by Dr. M. Filippov, Nizhny Novgorod, Russia, and Dr. D. Bruns, Homburg, Germany). In each case, CLC sequences were fused in-frame to the 5′ end of the coding sequences of enhanced green, monomeric cherry, or monomeric yellow fluorescence protein (eGFP, mCherry, or mYFP, respectively). Chimeric constructs were generated using overlapping PCR strategies.

For confocal images or cellular electrophysiology experiments, we transfected 1–2 μg of plasmid DNAs (CLC transporters and their chimeric proteins) into HEK293T cells either alone or in combination with fluorescent LAMP1 (a gift from Walther Mothes, Addgene plasmid 1817) (47), Rab7 (a gift from Richard Pagano, Addgene plasmid 12605) (48), or Bcl-2-Cb5 (a gift from Clark Distelhorst, Addgene plasmid 1800) (49) (0.1–0.2 μg of DNA encoding intracellular marker proteins) either using Lipofectamine 2000 (Invitrogen) or the calcium phosphate method. 24–36 h post-transfection, cells were used for experiments. For each construct, two independent recombinants from the same transformation were examined and shown to exhibit indistinguishable functional properties

For high-resolution clear native electrophoresis, we increased the molecular weight of ClC-3b by adding the coding region of MBP in-frame to its 3′ end using an overlapping PCR strategy. Point mutations N880Q and N883Q for MBP-ClC-3b and N428Q and N431Q for ClC-4 were inserted using an overlapping PCR strategy as well. We additionally attached a His_{10} tag sequence at the 5′ ends of the coding sequences of MBP-ClC-3b-eGFP as well as of ClC-4-mCherry for immobilized metal affinity chromatography purification when needed. HEK293T cells were transfected with 5 μg of FsY1.1 G.W./His_{10}-MBP-ClC-3b-eGFP or 5 μg of FsY1.1 G.W./His_{10}-ClC-4-eGFP alone or co-transfected with the two DNAs using the calcium phosphate method. In another set of experiments, 5 μg of FsY1.1 G.W./His_{10}-MBP-ClC-3b-eGFP and 5 μg of FsY1.1 G.W./His_{10}-ClC-4-mCherry were co-transfected to show the heterodimer in yellow because the fluorescences of eGFP and mCherry overlap. As a control, 4 μg of pSVL/mYFP hClC-1 was transfected. All experiments were performed 24 h after transfection. Normalized fluorescence intensities were calculated from co-expression experiments by dividing the fluorescence intensity of the ClC-3-eGFP homodimer, the ClC-4-eGFP homodimer, or the ClC-3-ClC-4 heterodimer band by the total fluorescence intensity measured in the gel lane.

Preparation of WT and Clcn3$^{-/-}$ astrocytes

Astrocytes were prepared from WT or *Clcn3*$^{-/-}$ (5) litter mates at postnatal day 1 after killing by decapitation. Hippocampi were dissected and mechanically dissociated to produce single cells by passing it through a 100-μm pore mesh. The cell suspension was centrifuged at 1500 $\times$ *g* for 10 min and resuspended in DMEM containing 10% FBS, 100 units/ml penicillin, and 100 μg/ml streptomycin (DM10 medium). The cells were then plated in 5-ml flasks precoated with 0.5 mg/ml of collagen, rat tail type II, and then cultured at 37 °C in a 95% air/5% CO_2 incubator. After growing to confluence (7–8 days), astrocytes were detached using trypsin-EDTA and collected by pelleting down using centrifugation (1500 $\times$ *g* for 10 min). Cell pellets were resuspended by careful pipetting using DM10 medium, plated on glass coverslips, and cultured at 37 °C in a 95% air/5% CO_2 incubator for 5 days more. One day after plating, cells were transduced using lentiviral particles and used for imaging 3–4 days later.

Lentiviral constructs and production

The coding region of ClC-4-mCherry or -eGFP was cloned in the pRRL.sin.cPPT.CMV.WPRE lentiviral transfer vector (50, 51). Lentiviral particles were performed as described previously (52). The transfer vector plasmid (P156rrL), the helper plasmids (pRSV-REV, pMDLg/pRRE, and the vesicular stomatitis virus G protein–expressing plasmid, kindly provided by Dr. Thomas Südhof) were co-transfected into HEK293FT cells using the calcium phosphate transfection method. After 14 h, the transfection medium was replaced with fresh medium (DMEM, 10% FCS, 100 mM sodium pyruvate, 100 mM non-

essential amino acids, and 100 mM GlutaMAX). 48 h later the virus was harvested, filtered (0.2-μm PVDF membrane, Millipore), and concentrated by ultracentrifugation. The viral particles were immediately frozen and stored at −80 °C. Lentiviral particles were added directly to the medium containing primary astrocytes.

Electrophysiology

Standard whole-cell patch clamp recordings were performed using an EPC-10 amplifier controlled by PatchMaster (HEKA, Germany) (2). Borosilicate pipettes (Harvard Apparatus) were pulled with resistances of 0.9–2.0 megaohm. Series resistance compensation and capacitance cancellation were applied, resulting in less than 5 mV voltage error. P/4 leak subtraction with a baseline potential of −30 mV was used to cancel linear capacitances (53). The standard external and internal recording solutions contained 160 mM NaCl, 15 mM HEPES, 4 mM potassium gluconate, 2 mM $CaCl_2$, and 1 mM $MgCl_2$ (pH 7.4) or 105 mM NaCl, 15 mM HEPES, 5 mM $MgCl_2$, and 5 mM EGTA (pH 7.4), respectively.

Confocal imaging and co-localization analysis

Images were acquired with a Leica TCS SP5 II inverted microscope (Leica, Wetzlar, Germany) using a ×63 oil immersion objective from living cells in PBS containing Ca^{2+} and Mg^{2+} (Gibco) at room temperature (22–24 °C). The plasma membrane marker CellMask™ (Invitrogen) was added to the culture medium before imaging according to the instructions of the manufacturer. eGPF, mRFP, or mCherry fluorophores were excited with a 488-nm argon laser, mRFP or mCherry with a 594-nm helium-neon laser, and CellMask™ at 633 nm. Emission signals were detected after filtering with 500- to 550-nm, 600- to 640-nm, and 640- to 700-nm bandpass filters, respectively. Confocal images were assembled for publication in ImageJ 1.44p software (National Institutes of Health, Bethesda, MD) (54).

Co-localization was quantified by calculating the MC using the JACoP plugin (55) embedded in the ImageJ 1.44p software (National Institutes of Health) (54). At least five different fields of view (containing at least three co-transfected cells each) for each construct from at least two independent co-transfections were analyzed. For all tested constructs, transfected cells exhibit rather homogenous levels of whole-cell fluorescence intensities, and we excluded cells from analysis that displayed either very low or very high expression levels upon visual inspection.

In experiments testing for ER localization of chimeric transporters, we co-expressed either calnexin-mCherry (56) or Bcl-2-eGFP (49), depending on the fluorescent protein to which the tested transporter was linked. We evaluated the equivalence of the marker proteins in co-expression experiments of calnexin-mCherry and eGFP-Bcl-2. Such experiments demonstrated perfect co-localization (MC = 0.99 ± 0.002, $n = 8$).

High-resolution clear native electrophoresis

Transfected HEK293T cells were washed with ice-cold phosphate-buffered saline and lysed in a buffer containing 0.1 M sodium phosphate (pH 8.0), 0.5% digitonin, protease inhibitors, and 20 mM iodoacetamide for 15 min and transferred into a reaction tube. After a clear spin at 4 °C, an aliquot of the resulting whole-cell lysate (approximately 10 μg) was loaded on a native gel. 4–14% acrylamide gradient gels were prepared as described previously (29, 30). The anode buffer contained 25 mM imidazole/HCl (pH 7.0) and cathode buffer (50 mM Tricine and 7.5 mM imidazole (pH 7.0)). Cathode buffer was supplemented with the anionic detergent sodium deoxycholate (0.04%) and the non-ionic detergent dodecyl maltoside (0.008%) (30). Gels were run in the cold (8 °C), and the original voltage was set to 100 V. After 1 h, the voltage was raised to 150 V. The electrophoresis was stopped after an additional 2 h.

Gels were scanned on a fluorescence gel scanner (Typhoon FLA 9500, GE Healthcare) at 100-μm resolution. eGFP and mYFP were excited at 473 nm, and their emission was recorded using a 530/20 bandpass filter. mCherry was excited at 532 nm, and the emission was recorded using a 575-nm long pass filter. Gel images were quantified using Fiji software as described previously (57). The two channel recordings were analyzed and quantified separately using the built-in tools for gel analysis.

Data analysis

Data analysis was performed using a combination of FitMaster (HEKA), Origin (OriginLab), SigmaPlot (Systat Software), and Excel (Microsoft) software. All data are presented as mean ± S.D., and statistical analysis was done by Student's and Mann-Whitney rank-sum test, with significance levels as follows: *, $p < 0.05$; **, $p < 0.01$; ***, $p < 0.001$.

Author contributions—R. E. G. and S. B.-P. planned, performed, and analyzed experiments and wrote the manuscript. A. F planned and performed experiments. C. F. planned experiments and wrote the manuscript.

Acknowledgments—We thank Dr. Thomas Jentsch for providing Clcn3$^{-/-}$ mice; Drs. Gustavo A. Guzman, Patricia Hidalgo, and Gabriel Stölting for helpful discussions; and Petra Thelen for excellent technical assistance.

References

1. Friedrich, T., Breiderhoff, T., and Jentsch, T. J. (1999) Mutational analysis demonstrates that ClC-4 and ClC-5 directly mediate plasma membrane currents. *J. Biol. Chem.* **274,** 896–902
2. Guzman, R. E., Grieschat, M., Fahlke, C., and Alekov, A. K. (2013) ClC-3 is an intracellular chloride/proton exchanger with large voltage-dependent nonlinear capacitance. *ACS Chem. Neurosci.* **4,** 994–1003
3. Kawasaki, M., Uchida, S., Monkawa, T., Miyawaki, A., Mikoshiba, K., Marumo, F., and Sasaki, S. (1994) Cloning and expression of a protein kinase C-regulated chloride channel abundantly expressed in rat brain neuronal cells. *Neuron* **12,** 597–604
4. van Slegtenhorst, M. A., Bassi, M. T., Borsani, G., Wapenaar, M. C., Ferrero, G. B., de Conciliis, L., Rugarli, E. I., Grillo, A., Franco, B., Zoghbi, H. Y., and Ballabio, A. (1994) A gene from the Xp22.3 region shares homology with voltage-gated chloride channels. *Hum. Mol. Genet.* **3,** 547–552
5. Stobrawa, S. M., Breiderhoff, T., Takamori, S., Engel, D., Schweizer, M., Zdebik, A. A., Bösl, M. R., Ruether, K., Jahn, H., Draguhn, A., Jahn, R., and Jentsch, T. J. (2001) Disruption of ClC-3, a chloride channel expressed on synaptic vesicles, leads to a loss of the hippocampus. *Neuron* **29,** 185–196
6. Dickerson, L. W., Bonthius, D. J., Schutte, B. C., Yang, B., Barna, T. J., Bailey, M. C., Nehrke, K., Williamson, R. A., and Lamb, F. S. (2002) Altered

GABAergic function accompanies hippocampal degeneration in mice lacking ClC-3 voltage-gated chloride channels. *Brain Res.* **958,** 227–250
7. Yoshikawa, M., Uchida, S., Ezaki, J., Rai, T., Hayama, A., Kobayashi, K., Kida, Y., Noda, M., Koike, M., Uchiyama, Y., Marumo, F., Kominami, E., and Sasaki, S. (2002) CLC-3 deficiency leads to phenotypes similar to human neuronal ceroid lipofuscinosis. *Genes Cells* **7,** 597–605
8. Hu, H., Haas, S. A., Chelly, J., Van Esch, H., Raynaud, M., de Brouwer, A. P., Weinert, S., Froyen, G., Frints, S. G., Laumonnier, F., Zemojtel, T., Love, M. I., Richard, H., Emde, A. K., Bienek, M., *et al. Mol. Psychiatr.* **21,** 133–148
9. Palmer, E. E., Stuhlmann, T., Weinert, S., Haan, E., Van Esch, H., Holvoet, M., Boyle, J., Leffler, M., Raynaud, M., Moraine, C., van Bokhoven, H., Kleefstra, T., Kahrizi, K., Najmabadi, H., Ropers, H. H., Delgado, M. R., *et al.* (2016) *De novo* and inherited mutations in the X-linked gene CLCN4 are associated with syndromic intellectual disability and behavior and seizure disorders in males and females. *Mol. Psychiatr.* 10.1038/mp.2016.135
10. Okkenhaug, H., Weylandt, K. H., Carmena, D., Wells, D. J., Higgins, C. F., and Sardini, A. (2006) The human ClC-4 protein, a member of the CLC chloride channel/transporter family, is localized to the endoplasmic reticulum by its N-terminus. *FASEB J.* **20,** 2390–2392
11. Mohammad-Panah, R., Ackerley, C., Rommens, J., Choudhury, M., Wang, Y., and Bear, C. E. (2002) The chloride channel ClC-4 co-localizes with CFTR and may mediate chloride flux across the apical membrane of intestinal epithelia. *J. Biol. Chem.* **277,** 566–574
12. Huang, L., Cao, J., Wang, H., Vo, L. A., and Brand, J. G. (2005) Identification and functional characterization of a voltage-gated chloride channel and its novel splice variant in taste bud cells. *J. Biol. Chem.* **280,** 36150–36157
13. Suzuki, T., Rai, T., Hayama, A., Sohara, E., Suda, S., Itoh, T., Sasaki, S., and Uchida, S. (2006) Intracellular localization of ClC chloride channels and their ability to form hetero-oligomers. *J. Cell. Physiol.* **206,** 792–798
14. Günther, W., Lüchow, A., Cluzeaud, F., Vandewalle, A., and Jentsch, T. J. (1998) ClC-5, the chloride channel mutated in Dent's disease, colocalizes with the proton pump in endocytotically active kidney cells. *Proc. Natl. Acad. Sci. U.S.A.* **95,** 8075–8080
15. Guzman, R. E., Miranda-Laferte, E., Franzen, A., and Fahlke, C. (2015) Neuronal ClC-3 splice variants differ in subcellular localizations, but mediate identical transport functions. *J. Biol. Chem.* **290,** 25851–25862
16. Gentzsch, M., Cui, L., Mengos, A., Chang, X. B., Chen, J. H., and Riordan, J. R. (2003) The PDZ-binding chloride channel ClC-3B localizes to the Golgi and associates with cystic fibrosis transmembrane conductance regulator-interacting PDZ proteins. *J. Biol. Chem.* **278,** 6440–6449
17. Maritzen, T., Keating, D. J., Neagoe, I., Zdebik, A. A., and Jentsch, T. J. (2008) Role of the vesicular chloride transporter ClC-3 in neuroendocrine tissue. *J. Neurosci.* **28,** 10587–10598
18. Guzman, R. E., Alekov, A. K., Filippov, M., Hegermann, J., and Fahlke, C. (2014) Involvement of ClC-3 chloride/proton exchangers in controlling glutamatergic synaptic strength in cultured hippocampal neurons. *Front. Cell. Neurosci.* **8,** 143
19. Alekov, A. K., and Fahlke, C. (2009) Channel-like slippage modes in the human anion/proton exchanger ClC-4. *J. Gen. Physiol.* **133,** 485–496
20. Zhao, Z., Li, X., Hao, J., Winston, J. H., and Weinman, S. A. (2007) The ClC-3 chloride transport protein traffics through the plasma membrane via interaction of an N-terminal dileucine cluster with clathrin. *J. Biol. Chem.* **282,** 29022–29031
21. Stauber, T., and Jentsch, T. J. (2010) Sorting motifs of the endosomal/lysosomal CLC chloride transporters. *J. Biol. Chem.* **285,** 34537–34548
22. Bateman, A. (2003) The structure of a domain common to archeabacteria and the homocysteine disease protein. *Trends Biochem. Sci.* **22,** 12–13
23. Meyer, S., and Dutzler, R. (2006) Crystal structure of the cytoplasmic domain of the chloride channel ClC-0. *Structure* **14,** 299–307
24. Meyer, S., Savaresi, S., Forster, I. C., and Dutzler, R. (2007) Nucleotide recognition by the cytoplasmic domain of the human chloride transporter ClC-5. *Nat. Struct. Mol. Biol.* **14,** 60–67
25. Krapivinsky, G., Gordon, E. A., Wickman, K., Velimirović, B., Krapivinsky, L., and Clapham, D. E. (1995) The G-protein-gated atrial K^+ channel IKACh is a heteromultimer of two inwardly rectifying K^+-channel proteins. *Nature* **374,** 135–141
26. Nothmann, D., Leinenweber, A., Torres-Salazar, D., Kovermann, P., Hotzy, J., Gameiro, A., Grewer, C., and Fahlke, C. (2011) Hetero-oligomerization of neuronal glutamate transporters. *J. Biol. Chem.* **286,** 3935–3943
27. Guzman, R. E., Schwarz, Y. N., Rettig, J., and Bruns, D. (2010) SNARE force synchronizes synaptic vesicle fusion and controls the kinetics of quantal synaptic transmission. *J. Neurosci.* **30,** 10272–10281
28. Nicke, A., Rettinger, J., Mutschler, E., and Schmalzing, G. (1999) Blue native PAGE as a useful method for the analysis of the assembly of distinct combinations of nicotinic acetylcholine receptor subunits. *J. Recept. Signal Transduct. Res.* **19,** 493–507
29. Wittig, I., Karas, M., and Schägger, H. (2007) High resolution clear native electrophoresis for in-gel functional assays and fluorescence studies of membrane protein complexes. *Mol. Cell. Proteomics* **6,** 1215–1225
30. Schmieder, S., Lindenthal, S., and Ehrenfeld, J. (2001) Tissue-specific *N*-glycosylation of the ClC-3 chloride channel. *Biochem. Biophys. Res. Commun.* **286,** 635–640
31. Fahlke, C., Knittle, T., Gurnett, C. A., Campbell, K. P., and George, A. L., Jr. (1997) Subunit stoichiometry of human muscle chloride channels. *J. Gen. Physiol.* **109,** 93–104
32. Detro-Dassen, S., Schänzler, M., Lauks, H., Martin, I., zu Berstenhorst, S. M., Nothmann, D., Torres-Salazar, D., Hidalgo, P., Schmalzing, G., and Fahlke, C. (2008) Conserved dimeric subunit stoichiometry of SLC26 multifunctional anion exchangers. *J. Biol. Chem.* **283,** 4177–4188
33. Fallah, G., Romer, T., tro Dassen, -S., Braam, U., Markwardt, F., and Schmalzing, G. (2011) TMEM16A (a)/anoctamin-1 shares a homodimeric architecture with CLC chloride channels. *Mol. Cell. Proteomics* **10,** M110
34. Falkenburger, B. H., Jensen, J. B., and Hille, B. (2010) Kinetics of M1 muscarinic receptor and G protein signaling to phospholipase C in living cells. *J. Gen. Physiol.* **135,** 81–97
35. Ronstedt, K., Sternberg, D., Detro-Dassen, S., Gramkow, T., Begemann, B., Becher, T., Kilian, P., Grieschat, M., Machtens, J. P., Schmalzing, G., Fischer, M., and Fahlke, C. (2015) Impaired surface membrane insertion of homo- and heterodimeric human muscle chloride channels carrying amino-terminal myotonia-causing mutations. *Sci. Rep.* **5,** 15382
36. Parkerson, K. A., and Sontheimer, H. (2004) Biophysical and pharmacological characterization of hypotonically activated chloride currents in cortical astrocytes. *Glia* **46,** 419–436
37. McMains, E., Krishnan, V., Prasad, S., and Gleason, E. (2011) Expression and localization of CLC chloride transport proteins in the avian retina. *PLoS ONE* **6,** e17647
38. Vanoye, C. G., and George, A. L., Jr. (2002) Functional characterization of recombinant human ClC-4 chloride channels in cultured mammalian cells. *J. Physiol.* **539,** 373–383
39. Hebeisen, S., Heidtmann, H., Cosmelli, D., Gonzalez, C., Poser, B., Latorre, R., Alvarez, O., and Fahlke, C. (2003) Anion permeation in human ClC-4 channels. *Biophys. J.* **84,** 2306–2318
40. Rugarli, E. I., Adler, D. A., Borsani, G., Tsuchiya, K., Franco, B., Hauge, X., Disteche, C., Chapman, V., and Ballabio, A. (1995) Different chromosomal localization of the *Clcn4* gene in *Mus spretus* and C57BL/6J mice. *Nat. Genet.* **10,** 466–471
41. Miller, C. (1982) Open-state substructure of single chloride channels from *Torpedo electroplax*. *Philos. Trans. R. Soc. Lond. B Biol. Sci.* **299,** 401–411
42. Zdebik, A. A., Zifarelli, G., Bergsdorf, E. Y., Soliani, P., Scheel, O., Jentsch, T. J., and Pusch, M. (2008) Determinants of anion-proton coupling in mammalian endosomal CLC proteins. *J. Biol. Chem.* **283,** 4219–4227
43. Robertson, J. L., Kolmakova-Partensky, L., and Miller, C. (2010) Design, function and structure of a monomeric ClC transporter. *Nature* **468,** 844–847
44. Chadda, R., Krishnamani, V., Mersch, K., Wong, J., Brimberry, M., Chadda, A., Kolmakova-Partensky, L., Friedman, L. J., Gelles, J., and Robertson, J. L. (2016) The dimerization equilibrium of a ClC Cl^-/H^+ antiporter in lipid bilayers. *eLife* **5,** e17438
45. Stauber, T., and Jentsch, T. J. (2013) Chloride in vesicular trafficking and function. *Annu. Rev. Physiol.* **75,** 453–477
46. Eggermont, J., Buyse, G., Voets, T., Tytgat, J., De Smedt, H., Droogmans, G., and Nilius, B. (1997) Alternative splicing of CIC-6 (a member of the CIC chloride-channel family) transcripts generates three truncated isoforms one of which, CIC-6c, is kidney-specific. *Biochem. J.* **325,** 269–276

47. Sherer, N. M., Lehmann, M. J., Jimenez-Soto, L. F., Ingmundson, A., Horner, S. M., Cicchetti, G., Allen, P. G., Pypaert, M., Cunningham, J. M., and Mothes, W. (2003) Visualization of retroviral replication in living cells reveals budding into multivesicular bodies. *Traffic* **4,** 785–801
48. Choudhury, A., Dominguez, M., Puri, V., Sharma, D. K., Narita, K., Wheatley, C. L., Marks, D. L., and Pagano, R. E. (2002) Rab proteins mediate Golgi transport of caveola-internalized glycosphingolipids and correct lipid trafficking in Niemann-Pick C cells. *J. Clin. Invest.* **109,** 1541–1550
49. Wang, N. S., Unkila, M. T., Reineks, E. Z., and Distelhorst, C. W. (2001) Transient expression of wild-type or mitochondrially targeted Bcl-2 induces apoptosis, whereas transient expression of endoplasmic reticulum-targeted Bcl-2 is protective against Bax-induced cell death. *J. Biol. Chem.* **276,** 44117–44128
50. Follenzi, A., Ailles, L. E., Bakovic, S., Geuna, M., and Naldini, L. (2000) Gene transfer by lentiviral vectors is limited by nuclear translocation and rescued by HIV-1 pol sequences. *Nat. Genet.* **25,** 217–222
51. Follenzi, A., Sabatino, G., Lombardo, A., Boccaccio, C., and Naldini, L. (2002) Efficient gene delivery and targeted expression to hepatocytes *in vivo* by improved lentiviral vectors. *Hum. Gene Ther.* **13,** 243–260
52. Barde, I., Salmon, P., and Trono, D. (2010) Production and titration of lentiviral vectors. *Curr. Protoc. Neurosci.* Chapter 4, Unit 4.21
53. Bezanilla, F., and Armstrong, C. M. (1977) Inactivation of the sodium channel: I: sodium current experiments. *J. Gen. Physiol.* **70,** 549–566
54. Ellgaard, L., and Helenius, A. (2003) Quality control in the endoplasmic reticulum. *Nat. Rev. Mol. Cell Biol.* **4,** 181–191
55. Bolte, S., and Cordelières, F. P. (2006) A guided tour into subcellular colocalization analysis in light microscopy. *J. Microsc.* **224,** 213–232
56. Schneider, C. A., Rasband, W. S., and Eliceiri, K. W. (2012) NIH Image to ImageJ: 25 years of image analysis. *Nat. Methods* **9,** 671–675
57. Stölting, G., Bungert-Plümke, S., Franzen, A., and Fahlke, C. (2015) Carboxy-terminal truncations of ClC-Kb abolish channel activation by barttin via modified common gating and trafficking. *J. Biol. Chem.* **290,** 30406–30416